Engineered Science

RESEARCH PAPER View Article Online

Doughnut-Structured FeS_2@C Nanorings: Towards the Efficient Synthesis and Application in High-Performance Li-ion Cathode

Qunbin Zhang, Jinyan Dai, Min Liao, Tao Duan and Weitang Yao*

Lithium-FeS_2 battery has the prospect of sustainable and low cost application. Nevertheless, the realization of high capacity and cyclic stability is still a huge challenge. To solve the problems of FeS_2 as a cathode material, such as the unstable structure and poor electronic conductivity, the eco-friendliness doughnut-structured FeS_2@C nanorings have been successfully synthesized in this work. When used as a cathode material for lithium-ion batteries (LIBs) (1-3 V), the doughnut-structured FeS_2@C nanorings can maintain the discharge capacity of 688.11 mAh g^{-1} after 100 cycles at the current density of 200 mA g^{-1}, showing excellent cyclic stability and capacity retention. More importantly, even under the high current density of 2 A g^{-1}, they still maintain average specific discharge capacity of 380.36 mAh g^{-1} after 500 cycles, showing a long cycle life. Furthermore, they have fairly excellent discharge energy density at the material level (~1040.21Wh/kg-FeS_2) after 100 cycles at a current density of 0.2 A g^{-1}. All the results show that our prepared doughnut-structured FeS_2@C nanorings cathode materials have a great application potential in LIBs.

Keywords: Doughnut-structured FeS_2@C nanorings; Cathode; Rate performance; Lithium-ion batteries

Received 28 November 2018**, Accepted** 23 January 2019

DOI: 10.30919/es8d728

1. Introduction

Owing to the rapid development of the social economy, environmental pollution and energy shortage are becoming more and more serious. Excellent and viable batteries are pressingly needed for multitudinous broaden beyond small electronic devices to large electric power storage equipments. The relatively mature lithium-ion batteries (LIBs), as a kind of clean and reliable storage device, are popular in various electric vehicles, stationary energy storage and portable electronic devices, etc.[1-3]Thus far, great progress has been made in the exploration of anode materials for LIBs, but the research on cathode materials has made relatively few achievements.[4] Therefore, developing advanced cathode materials with superior electrochemical performance is of vital significance.[5] It has been generally accepted that transition metal sulfides (TMS) have better capacity than conventional cathode materials.[6] Moreover, Studies have shown that the M-S ionic bonds are comparably weaker than M-O bonds, which is favorable for the electrochemical reversibility of TMS compared with transition metal oxides (TMO).[7] Over the past few decades, a large number of low-cost iron based reversible cathode materials have attracted considerable attention. These materials (e.g., FeF_3 and FeS_2) might replace typical $LiTMO_2$ intercalation cathodes, because they have the advantages of higher theoretical energy density and lower cost.[8-13] In particular, FeS_2 has attracted increasing attention owing to the abundance and eco-friendliness of Fe and S resources. In addition, pyrite (FeS_2) has mixed valence and intrinsic metal characteristics, which are favourable for its use in LIBs.[14]Corresponding to the formation of metal Fe^0 and insulating Li_2S ($FeS_2 + 4Li^+ + 4e^- \rightarrow Fe + 2Li_2S$),[9-13] the high theoretical capacity (894 mAh g^{-1}) of FeS_2 is more than three times of the current intercalation $LiNi_xCo_yMn_zO_2$ cathode (about 274 mAh g^{-1}).[15]

However, FeS_2 is usually hindered by large volume changes, low conductivity, and other factors, which make its poor electrochemical reversibility, and is difficult to use for commercial rechargeable LIBs. On one hand, the highly reactive nano-Fe^0 and high-resistance Li_2S produced after the first lithiation might seriously affect the reversibility of the lithium-ion battery.[16, 17] On the other hand, more complex products, including orthorhombic FeS_2, FeS_y and sulfur, were obtained after the first delithiation.[18] The charge transfer and ion diffusion of Li_2S and sulfur are slow, leading to high-resistance, poor rate performance and low reversibility.[19, 20] In addition, the presence of sulfur leads to the appearance of the notorious lithium polysulfide (Li_2S_x, $4 < x < 8$) and that will further harm the service life and capacity of LIBs.[21-24] Many effective schemes have been developed to solve these problems, including development of uniform FeS_2 nanostructure and composite FeS_2 electrode through microstructural engineering, C/conductive polymer coatings, etc.[16, 25-33] In particular, the inclusion of electrode materials with uniform size into conductive coating can not only promote the rapid intercalation and deintercalation of lithium ions, but also prevent the excessive reunion and coarsening of small metal nanoparticles, thus improving the cycling performance.[16, 25, 26]

Herein, we successfully synthesized unique doughnut-structured FeS_2@C nanorings as a cathode material for LIBs. Firstly, we chose a simple one-step hydrothermal method to obtain uniform α-Fe_2O_3 nanorings.[34] After coating with resorcinol formaldehyde (RF) via a sol-

Fundamental Science on Nuclear Wastes and Environmental Safety Laboratory, Sichuan Civil-military Integration Institute, Southwest University of Science and Technology, Mianyang, Sichuan, 621010, China

***E-mail:** wtyao@ustc.edu.cn*

gel process, α-Fe_2O_3 nanorings were converted into doughnut-structured Fe_3O_4@C nanorings by carbothermal reduction. These homogeneous Fe_3O_4@C nanorings can be completely converted to doughnut-structured FeS_2@C nanorings after sulfuration. The carbon layer structure profited from RF is beneficial for FeS_2 maintaining relatively stable nanostructure in discharge/charge processes. What's more, the carbon layer structure can also significantly improve the conductivity of materials and accelerate the electrochemical reaction. Therefore, these doughnut-structured FeS_2@C nanorings exhibit excellent electrochemical properties.

2. Experimental

2.1 Synthesis of α-Fe_2O_3 nanorings

The Fe_2O_3 nanorings were synthesized through a hydrothermal method using $NaH_2PO_4 \cdot 2H_2O$ and Na_2SO_4 as additives and $FeCl_3 \cdot 6H_2O$ as the iron source.[34] Specifically, 5.4057 g of $FeCl_3 \cdot 6H_2O$, 0.0250 g of $NaH_2PO_4 \cdot 2H_2O$ and 0.0781 g of Na_2SO_4 were dissolved in 1 L deionized water. Then the solution was transferred into a 100mL reactor and heated for 48 hours at 220 °C. After washing and drying, Fe_2O_3 nanorings red powder can be obtained.

2.2 Synthesis of Fe_3O_4@C nanorings

0.15 g of Fe_2O_3, 0.46 g of cetyltrimethylammonium bromide and 14.10 mL of H_2O were added to a flask. After stirring for an hour, 0.7 g of resorcinol (R), 57 mL of absolute ethanol and 0.2 mL of ammonia were added to the flask in turn. Subsequently, after stirring for 30 minutes, 0.1 mL of formalin (F) was finally added. The mixture was continuously stirred for 6 hours and then placed for half a day. After washing and drying, the Fe_2O_3@RF was obtained, and Fe_3O_4@C nanorings were prepared by heattreatment of Fe_2O_3@RF at 600 °C for 2 h in an N_2 atmosphere.

2.3 Synthesis of doughnut-structured FeS_2@C nanorings

Firstly, a mixture of Fe_3O_4@C nanorings and sulfur with the mass ratio of 1:1.1, was sealed into the vacuum quartz tube. Specifically, kept the quartz tube at 155 °C for 2 h and then raised the temperature to 550 °C for 2 h. After cooled naturally, the black powder was washed with carbon disulfide to remove excess sulfur to obtain doughnut-structured FeS_2@C nanorings.

2.4 Structural characterization

Scanning electron microscope (SEM) was performed using a Zeiss UItra 55 field emission scanning electron microscope. TEM, HRTEM, HAADF-STEM distribution analysis and EDX element mapping analysis were carried out on a Zeiss Libra200 FE. The phase of the material was studied by powder X-ray diffraction (XRD) patterns by a X' Pert pro. The test range was 3° – 80° at a scan rate of 1° min^{-1}. Thermogravimetric analysis (TGA) was performed using on a SQT-600 thermogravimetry analyzer from 25 °C to 750 °C under an air atmosphere with a heating rate of 5 °C min^{-1}. X-ray photoelectron spectra (XPS) was carried out on an ESCA Lab MKΠ X-ray photoelectron spectrometer. Raman spectra analysis was carried out on a Renishaw In Via confocal Raman microscope.

2.5 Electrochemical measurements

Active materials (80wt%), acetylene black (10wt%), and polyvinylidene fluorides(PVDF) (10wt%) were dispersed in N-methylpyrrolidino (NMP), placed a in mortar and ground until blended. Then the homogenate was evenly coated on a circular Al foil with a diameter of about 14mm.The electrolyte is composed of a mixture of 1, 3-dioxolane (DOL) and diglyme (DME) with volume ratio of 1:1 and 1 M lithium bis-trifluoromethanesulfonylimide (LiTFSI). The galvanostatic charge-discharge performance were tested on NEWARE battery-test system, with voltage ranges from 1.0 to 3.0 V at room temperature. Electrochemical performances including cyclic voltammetry (CV) and electrochemical impedance spectra (EIS) were tested on a VersaSTAT4. CV test conditions are with potentials ranges from 1 to 3 volts and at the scan rate of 0.1 mV s^{-1}. All tests were performed at room temperature.

3. Results and discussion

Fig. 1a shows the schematic illustration of the preparation process for doughnut-structured FeS_2@C nanorings. Firstly, the uniform -Fe_2O_3nanorings (Fig. 2a and 2b) were facilely obtained *via* a one-pot double anion-assisted (SO_4^{2-}, PO_4^{3-}) hydrothermal method. Secondly, Fe_2O_3@RF nanorings were fabricated by coating with resorcinol formaldehyde (RF) through a sol-gel process. Thirdly, the RF was carbonized into amorphous carbon under high temperature. Meanwhile, the Fe^{3+} ions in Fe_2O_3@C were reduced by the amorphous carbon on the surface of Fe_2O_3@C nanorings during carbothermal reduction, and the Fe_2O_3@C were converted into the Fe_3O_4@C. Finally, the uniform doughnut-structured FeS_2@C nanorings were fabricated *via* sulfuration (Fig. 1b) strategy. There was a very important step, Fe_3O_4-S@C hybrid nanorings were fabricated by impregnating sulfur reactants into the voids of Fe_3O_4@C nanorings by melt diffusion method. The fantastic doughnut-like structure of the uniform Fe_3O_4@C nanorings play a vital role in this strategy. The Fe_3O_4@C nanorings have larger specific surface area, which can accelerate the sulfidation reaction. The reaction (eq 1) in the sulfidation process is as follows:

$$Fe_3O_4 + 8S \xrightarrow{550\,^{\circ}C} 3FeS_2 + 2SO_2\uparrow \quad (1)$$

As a contrast, pristine FeS_2 (Fig. S2) was prepared by direct sulfidation of α-Fe_2O_3 nanorings.

Scanning electron microscopy (SEM) image (Fig. 2a) and transmission electron microscopy (TEM) image (Fig. 2b) clearly display that α-Fe_2O_3 nanorings exhibit a uniform ring shape. XRD pattern (Fig. 2c) of α-Fe_2O_3 nanorings matches well with the standard diffraction pattern (JCPDS 79-1741), indicating that the α-Fe_2O_3 nanorings have high purity and good crystallinity.[34] Similarly, the structural feature of doughnut-like-shaped Fe_3O_4@C nanorings can be clearly displayed by SEM (Fig. 2d). And the TEM image (Fig. 2e) shows that the inner Fe_3O_4 nanorings are about 150 nm in diameter and the thickness of carbon layer is about 10 nm. Meanwhile, it is worth noting that nano-scale materials have large specific surface area and can further improve the chemical reaction reactivity.[35] All peaks in XRD pattern (Fig. 2f) can be assigned to cubic-Fe_3O_4 (JCPDS 19-0629) without any detectable crystalline impurity. The strong characteristic peaks demonstrate the high crystallinity nature of the products. In addition, in order to analyze the bonding relationship more accurately, X-ray photoelectron spectroscopy (XPS, Fig. S1) measurement was also applied to investigate the Fe_3O_4@C nanoring. XPS spectrum (Fig. S1a) can provide a direct evidence for the presence of Fe, O, and C in Fe_3O_4@C nanorings. The characteristic peaks in Fig. S1a at binding energies of 287.7 , 531.1, and 710.5eV are related to C1s, O1s and Fe2p, respectively.[36] The chemical states of Fe, O, and C are further analyzed by high-resolution XPS spectroscopy (Fig. S1b, c and d). As shown in the Fig. S1b, the peaks located at 710.5 and 724.5 eV are associated with $Fe2p_{3/2}$ and $Fe2p_{1/2}$, respectively, which confirm the existence of Fe_3O_4.[36-38] The high-resolution O1s XPS spectrum (Fig. S1c), can be de-convoluted into four component peaks at 529.8, 531.1, 531.8 and 532.9

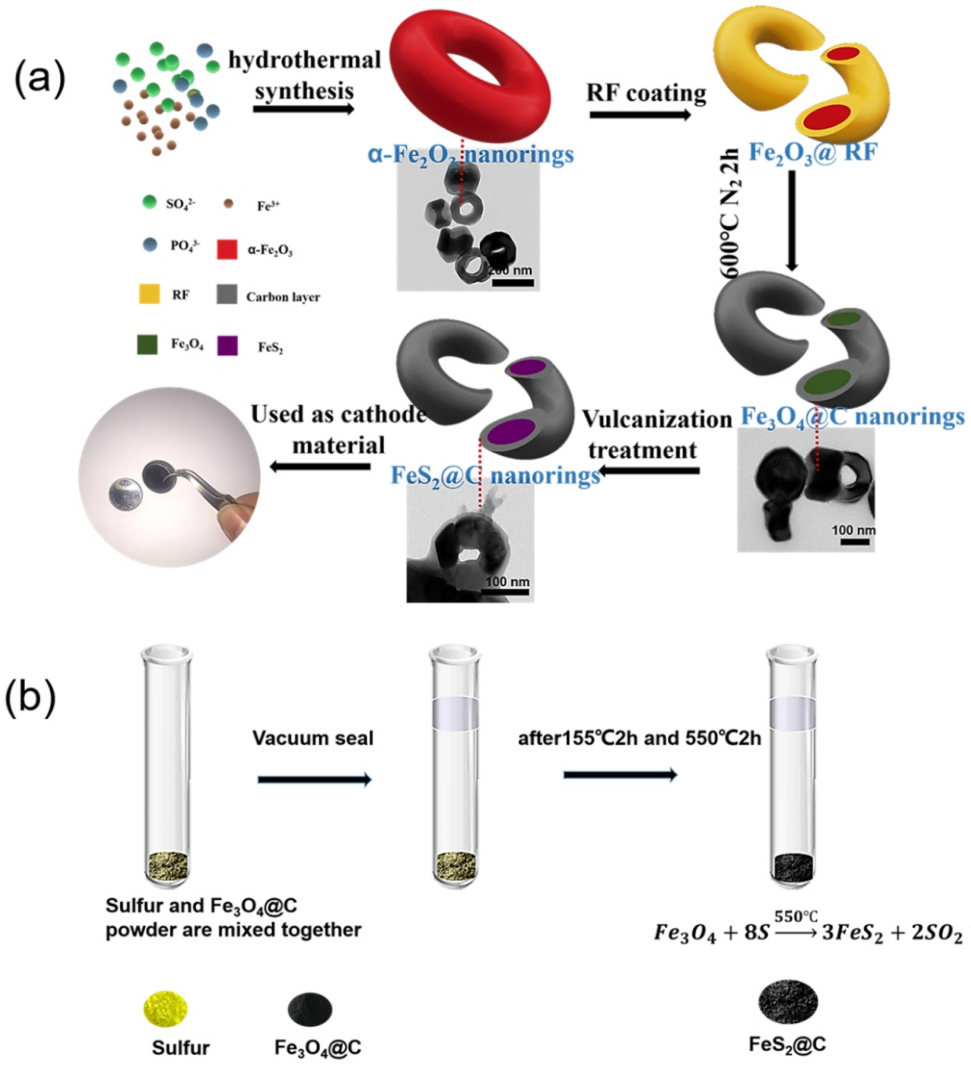

Fig. 1 (a) Schematic diagram for the preparation of doughnut-structured FeS_2@C nanorings cathode materials; (b) Schematic illustration of the sulfidation process for preparing doughnut-structured FeS_2@C nanorings.

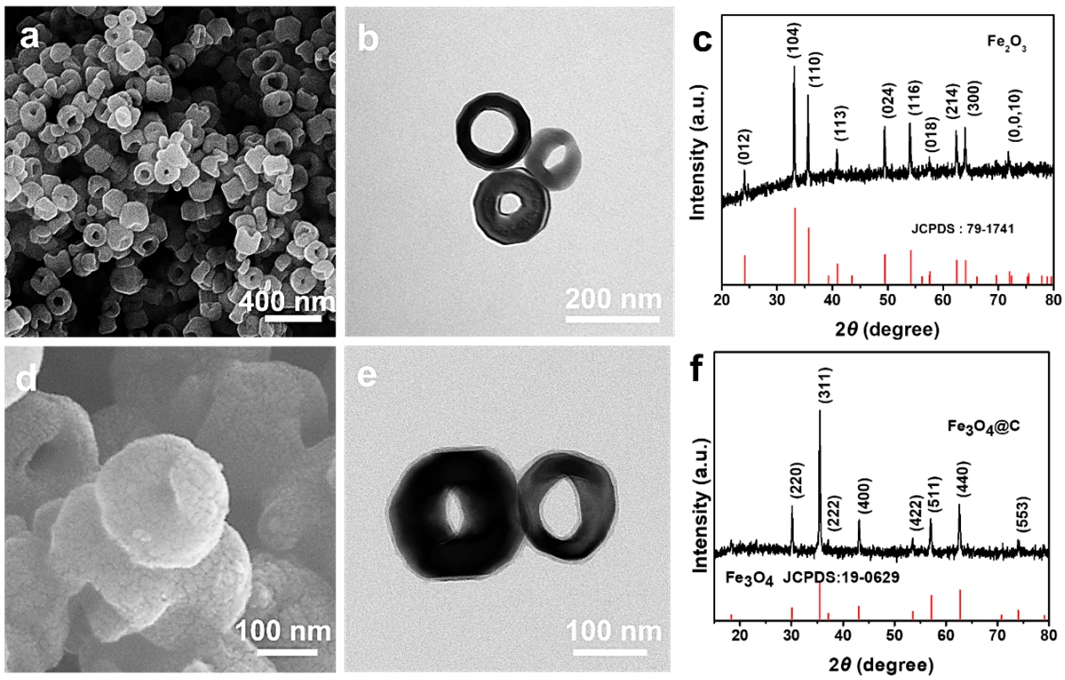

Fig. 2 (a) High-resolution SEM diagram of α-Fe_2O_3 nanorings with an average diameter of about 150 nm; (b) TEM image of typical α-Fe_2O_3 nanorings; (c) XRD pattern of well-crystallized typical α-Fe_2O_3 nanorings; (d) SEM diagram of Fe_3O_4@C nanorings with a diameter of about 150-200 nm; (e) TEM image of the typical Fe_3O_4@C nanorings. (f) XRD pattern of the typical Fe_3O_4@C nanorings in comparison with reference diffractogram of cubic-Fe_3O_4.

eV, corresponding to Fe-O-Fe, Fe-O, Fe-O-C, and C-O, respectively.[36, 39, 40] For the XPS spectrum of C1s (Fig. S1d), it can be further differentiated into three peaks located at 284.7, 286.0 and 288.9 eV, which are related to C-C and C=C, C-O and O-C=O, respectively.[41, 42]

In Fig. 3a, the doughnut-structured FeS_2@C nanorings are about 150-200 nm in diameter, and each nanoring gathers together by the electrostatic interaction. Fig. 3b shows the FeS_2@C nanorings SEM at high magnification and a broken nanoring (pink circle) was found. EDX spectrum of this area reveals that the product is composed of C, Fe and S. The mass fraction of carbon, iron and sulfur are about 11.55%, 46.16% and 42.29%, respectively. TEM image (Fig. 3c) further indicates that the doughnut-structured nanorings inherit the morphology and dimension of Fe_3O_4@C nanorings. The diameter of the nanorings is about 150 nm and the nanorings are encapsulated uniformly by carbon

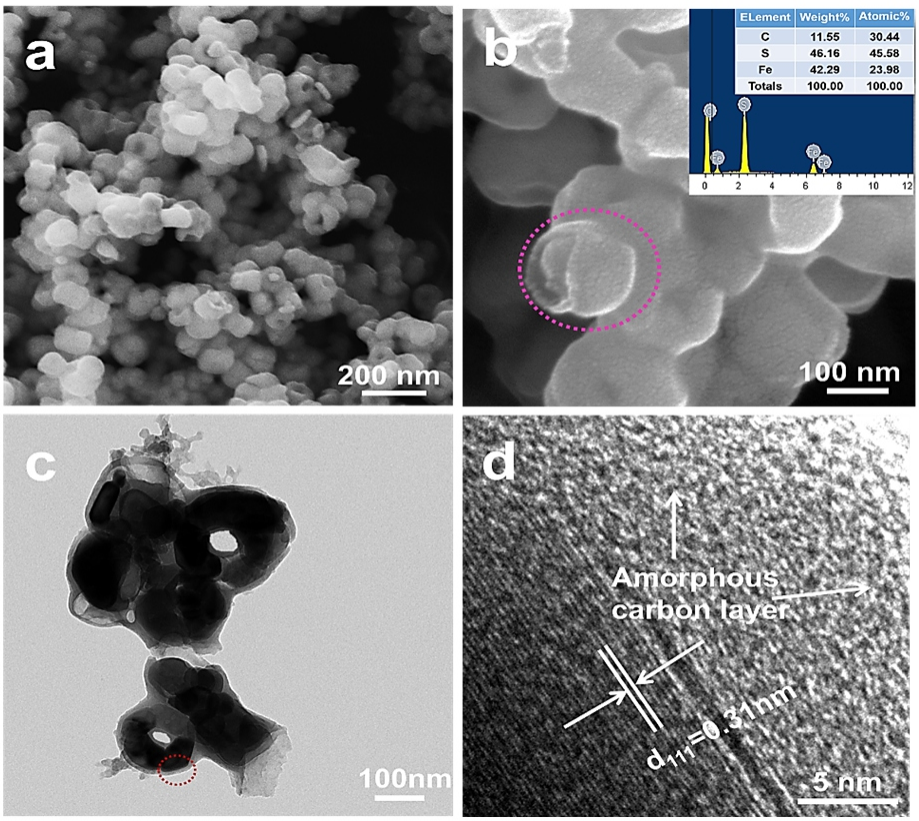

Fig. 3 (a) SEM image of uniform doughnut-structured FeS_2@C nanorings; (b) The high magnification SEM image of uniform doughnut-structured FeS_2@C nanorings, inset is the EDX spectrum of the selected section;(c) TEM image of typical doughnut-structured FeS_2@C nanorings; (d) HRTEM corresponding to the high magnification TEM image of doughnut-structured FeS_2@C nanorings.

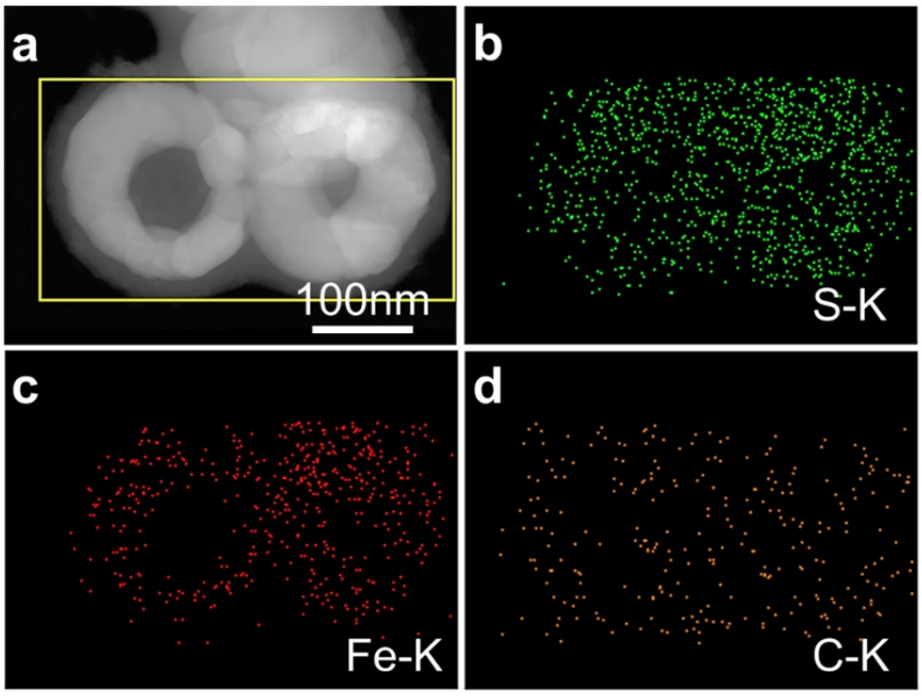

Fig. 4 HAADF-STEM distribution analysis of the typical doughnut-structured FeS_2@C nanorings; (a) TEM image, and EDX elemental mappings of (b) S, (c) Fe and (d) C.

shell (about 10 nm). The relatively suitable carbon layer may prevent the destruction of internal active substances and relieve larger volume changes, thus making the electrochemical reaction more stable. Meanwhile, nano-scale particle size is more conducive to the rapid progress of electrochemical reaction. To more clearly describe the microstructure of the FeS_2@C nanorings, HRTEM was employed. HRTEM image (Fig. 3d) shows obvious lattice fringes, and the interplanar distance is 0.31 nm, corresponding to the (111) plane of FeS_2. As shown in Fig. 4 and Fig. S3, the elements Fe (red), S (green), and C (yellow) are uniformly distributed on the selected doughnut-structured FeS_2@C nanorings.

Fig. 5a shows the Powder X-ray diffraction patterns of the as-synthesized pristine FeS_2 and doughnut-structured FeS_2@C nanorings. The characteristic diffraction peaks corresponding to pristine FeS_2 and FeS_2@C nanorings match well with the standard cubic phase FeS_2 (JCPDS 42-1340) with a spatial group *Pa-3* (205),[43] which correspond to pyrite FeS_2. The diffraction peaks of the XRD pattern of both pristine FeS_2 and FeS_2@C nanorings are very sharp, indicating that they are well-crystallized. There is not much difference in diffraction peaks between pristine FeS_2 and doughnut-structured FeS_2@C nanorings. Fig. 5b shows the Raman spectra of the pristine FeS_2 and doughnut-structured FeS_2@C nanorings, respectively. The peaks situated at 336,

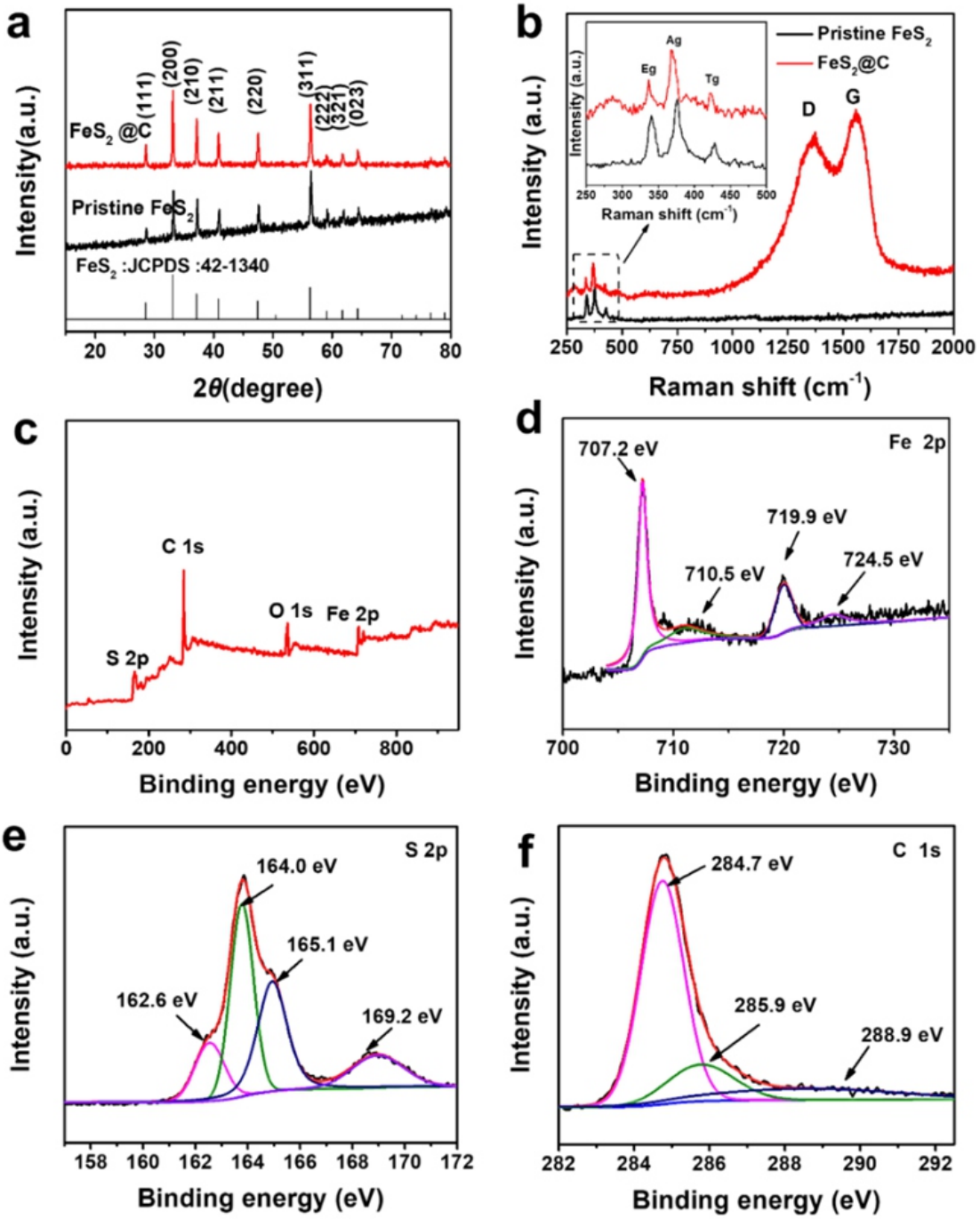

Fig. 5 (a) XRD pattern of pristine FeS_2 and doughnut-structured FeS_2@C nanorings in comparison with reference diffractogram of cubic phase FeS_2; (b) Raman spectra of pristine FeS_2 and FeS_2@C nanorings ;The XPS spectra of doughnut-structured FeS_2@C nanorings (c) survey; (d) Fe 2p; (e) S 2p; (f) C 1s.

370 and 423 cm^{-1} correspond to Eg, Ag, and Tg modes of FeS_2 crystals, respectively.[43-46] By comparing with pristine FeS_2, the two characteristic peaks located at 1360 cm^{-1} (disorder-induced D band) and 1560 cm^{-1} (graphitic G band) in Fig. 5b also authenticate the existance of carbon in the doughnut-structured FeS_2@C nanorings. After calculation, the intensity ratio of D and G band (I_D/I_G) is 0.904, indicating that the graphitized amorphous carbon formed on nanorings surface.[47] As we all know, graphitized carbon can improve electrical conductivity and promote electrons transportation.

In order to understand the specific amount of active materials，we carried out the thermogravimetric analysis (TGA) of doughnut-structured FeS_2@C nanorings (Fig. S4). It is supposed that the thermogravimetric test is mainly divided into three processes,[48] including the evaporation of adsorbed water, oxidation of carbon (eq. S1) and oxidation of pyrite (eq. S2). According to Fig. S4, it is known that the mass of the sample is almost not reduced (28 – 200 °C). Thus, the content of adsorbed water is ignored. The initial weight loss of the sample is attributed to the oxidation of amorphous C (200 – 480 °C). The second reduction in the sample weight is attributed to the oxidation of FeS_2 to Fe_2O_3 (480 – 650 °C). The final residue is Fe_2O_3 (~58.5%). According to the results of TGA, it is deduced that FeS_2 in doughnut-structured FeS_2@C nanorings is about 87.75% and the carbon content is about 12.25%, which is roughly the same as the EDX results. (Inset of Fig. 3b). To determine the chemical structure of doughnut-structured FeS_2@C nanorings, XPS was also carried out. As shown in the full scan spectrum (Fig. 5c), the sharp peaks at 162.6, 284.7 and 707.2 eV are allocated in peaks of S2p, C1s and Fe2p, respectively.[49] In the high-resolution Fe2p XPS spectrum (Fig. 5d), this peak could be identified as consisting of four component peaks at 707.2, 710.5, 719.9 and 724.5 eV. The peak of 710.5 eV is attributed to Fe $2p_{3/2}$, and the peaks at 719.9 and 724.5 eV are associated with Fe $2p_{1/2}$.[26, 36, 50] Moreover, the spin energy separation between 719.9 and 707.2 eV is 12.7 eV, conforming to the typical characteristic of FeS_2 spectra.[51] The S2p signal (Fig. 5e) displays one peak corresponding to $S2p_{3/2}$ (162.6 eV), which is related to FeS_2.[32] The peaks of 165.1 and 164 eV can be attributed to S_x^{2-}[33, 52].The peak of 169.2 eV is attributed to oxidized sulfur species (e.g., SO_x).[53] The C1s spectrum of doughnut-structured FeS_2@C nanorings in Fig. 5f consists of three peaks at binding energies of 284.7, 285.9 and 288.9eV, related to C-C and C=C, C-O and O-C=O, respectively.[54, 55]

Lithium storage properties of doughnut-structured FeS_2@C nanorings are studied in a button-shape half-cell using lithium as a reference electrode. In particular, it should be pointed out that the carbon contained in the doughnut-structured FeS_2@C nanorings can't provide capacity under the working condition of 1.0-3.0 V.[36] The representative cyclic voltammetry (CV) curves of doughnut-structured FeS_2@C nanorings for the first three cycles in the range of 1.0 to 3.0 V at a scan rate of 0.1 mV s^{-1} are shown in Fig. 6a. For the first cycle of doughnut-structured FeS_2@C nanorings, three oxidation peaks at about 1.84, 2.2, and 2.5 V can be clearly observed in CV curve, while a big reduction peak is at about 1.24 V. According to relevant reports,[6, 56] theoretically, two reduction peaks should appear during the first discharge process. In detail, the reduction peaks are related to the conversion of FeS_2 into Li_2S and Fe^0 during the first cycle. However, the lithiation (eq 2) and conversion (eq 3) reactions are basically occurring at the same time. Their potentials are very close and usually overlap with each other, thus coming into being only a strong cathodic peak(~1.24 V) during the first discharge process.[6, 36]

$$FeS_2 + 2Li^+ + 2e^- \rightarrow Li_2\ FeS_2 \quad (2)$$

$$Li_2FeS_2 + 2Li^+ + 2e^- \rightarrow Fe + 2Li_2S \quad (3)$$

$$Fe + 2Li_2S \rightarrow Li_2FeS_2 + 2Li^+ + 2e^- \quad (4)$$

$$Li_2FeS_2 \rightarrow Li_{2-x}FeS_2 + xLi^- + xe^- (0.5 < x < 0.8) \quad (5)$$

$$Li_{2-x}FeS_2 \rightarrow 0.8ortho - FeS_2 + 0.2FeS_{8/7} + 0.175S + (2-x)Li^+ + (2-x)e^- \quad (6)$$

Starting from the second cycle, since *ortho*-FeS_2 and S are proposed as charge products in FeS_2 electrodes, it is predicted that the discharges will abide by a slightly different mechanism.[6] Fig. 6b clearly shows the charge-discharge curves of the doughnut-structured FeS_2@C nanoring electrode in the first three circles at 100 mA g^{-1}. In the first discharge process, the electrode has a long voltage platform close to 1.50 V, but the voltage platform decreases gradually in the subsequent cycles. Particularly, in the first charge process, there is another voltage platform at about 2.50 V, but it disappears in the subsequent cycles. The difference of voltage platform between the first circle and the other two circles can be attributed to a slightly different charge and discharge mechanism.[10, 36] The initial charge and discharge capacity of doughnut-structured FeS_2@C nanoring electrode is 848.74 and 904.95 mAh g^{-1}, respectively, and the irreversible capacity loss is about 56.21 mAh g^{-1}. The loss might be due to the incomplete dissolution of Li_2S and SEI film.[25, 43, 57] For doughnut-structured FeS_2@C nanoring electrode, the initial Coulombic efficiency is 93.8% and the Coulombic efficiency of the second cycle and third cycle is 98.17% and 99.3%, respectively. In addition, the almost overlapped charge and discharge curves of FeS_2@C at the 2nd and 3rd cycle also evidenced its better reversibility. Fig. 6c shows the charge and discharge curves of the 100th cycle from the doughnut-structured FeS_2@C nanoring electrode at the current densities of 100 and 200, 400, 600, 800, 1000 and 2000 mA g^{-1}. After 100 cycles, doughnut-structured FeS_2@C nanoring electrode can still reach the discharge capacity of 765.85, 688.11, 564.37, 545.17, 516.05, 478.28 and 411.69 mAh g^{-1}, respectively, although the charge-discharge curves at different current densities have slight changes (the voltage platform slightly decreases under different current densities).[58]

Addition to the high capacity and good cycling stability, the rate capability performance is also a significant indicator to evaluate the quality of electrode materials. The rate performance of the doughnut-structured FeS_2@C nanorings electrode was tested at a current density of 0.1–2 Ag^{-1} (Fig. 6d). At the rate capability performance test, the initial Coulombic efficiency at different current densities is 95.61%,86.74%, 90.44%, 94.47%, 96.28%, 92.82% and 86.58%, respectively. Even under the very high current density of 2 A g^{-1}, the doughnut-structured FeS_2@C nanoring electrode can maintain a relatively high average discharge capacity (424.27 mAh g^{-1}), showing a good capacity retention rate. It is worth noting that after the high rate charge-discharge cycles, when the current density is changed to 0.1 A g^{-1} again, the average discharge capacity can still reach 772.13 mAh g^{-1}. This indicates that the doughnut-structured FeS_2@C nanorings electrode has excellent structural stability. The same conclusion can be obtained based on the SEM images (Fig. 7) of the doughnut-structured FeS_2@C nanorings after the rate capability performance test. The doughnut-like structure is basically not destroyed, which means that the doughnut-structured FeS_2@C nanorings have excellent structural stability. Carbon shell can inhibit further agglomeration and coarsening of doughnut-structured FeS_2@C nanorings, and help to store more Li ions.

Fig. 6e gives the cyclic capacity diagram of the first 100 cycles of the doughnut-structured FeS_2@C nanorings battery at the current density of 200 mA g^{-1}. The initial Coulombic efficiency is only 90.58%. After 100 cycles, there is almost no capacity degradation, showing good cycling performance, which might be attributed to stable carbon shell

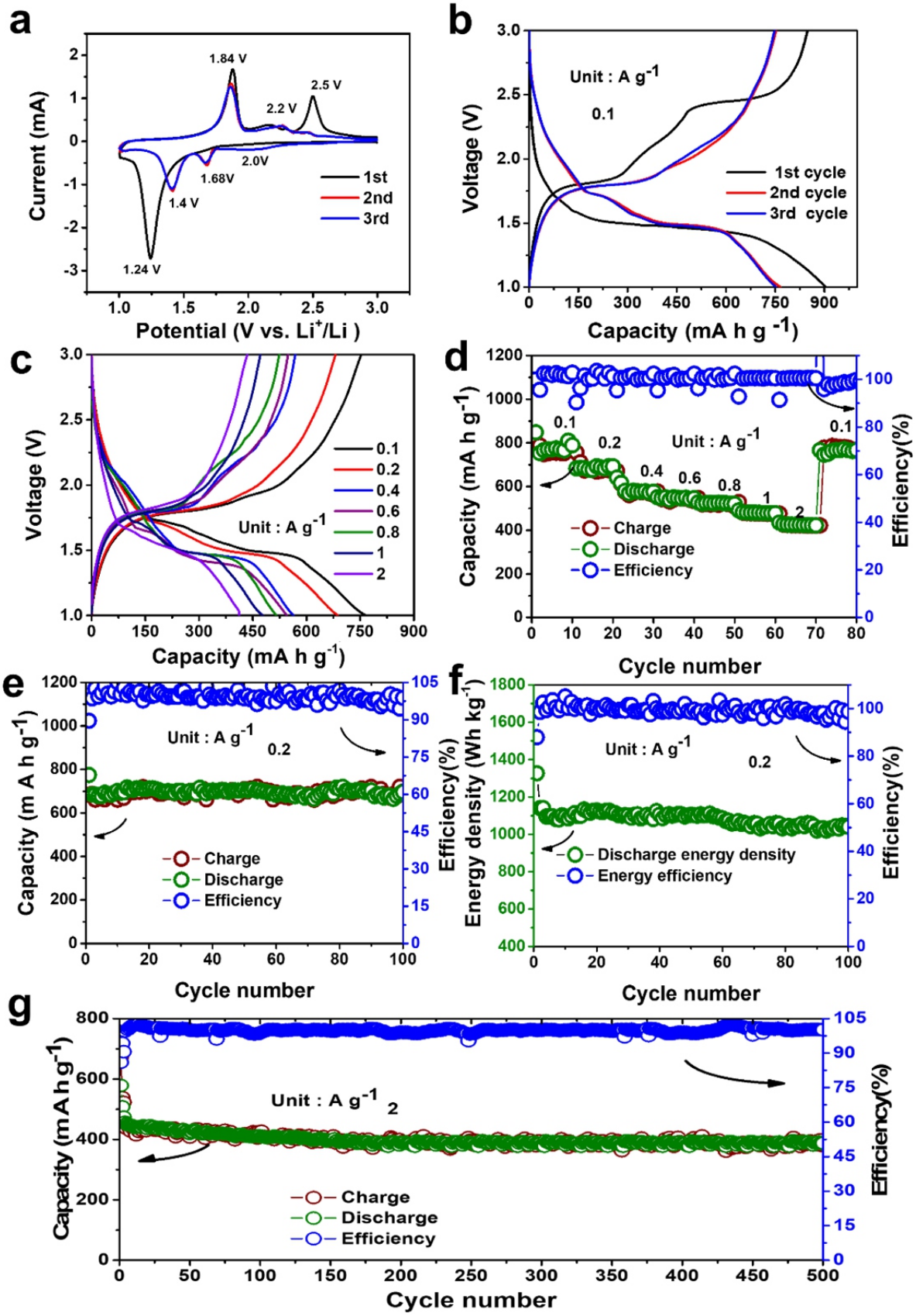

Fig. 6 (a) CV curves at a scanning rate of 0.1 mV s^{-1} in the voltage range of 1.0-3.0 V; (b) The voltage-capacity curves at 0.1 A g^{-1}; (c)Voltage-capacity curves of doughnut-structured FeS_2@C nanoring electrode at different rates (from 0.1 to 2 A g^{-1}); (d) Rate capability performance at different rates (from 0.1 to 2 A g^{-1}); (e) Cycling performance of doughnut-structured FeS_2@C nanorings cathode at 0.2 A g^{-1}; (f) Discharge energy density vs. cycle number at the material level (~Wh/kg-FeS_2); (g) Long cycling performance of doughnut-structured FeS_2@C nanorings after 500 cycles at a current density of 2 A g^{-1}.

structure. Compared with the pristine FeS_2 (Fig. S5), the FeS_2@C electrode can maintain a discharge capacity of 688.11 mAh g^{-1} from its initial value of 764.25 mAh g^{-1} after 100 cycles, while for pristine FeS_2, its discharge capacity decreases quickly from 571.71 to 350.78 mAh g^{-1} after 100 cycles with the corresponding capacity retention of 61.35%. Therefore, it is believed that the stable carbon shell structure is an effective way to prevent rapid capacity fading and improve the electrochemical performance of FeS_2. The discharge energy density (eq S3) of the doughnut-structured FeS_2@C nanoring electrode initially reached 1327.01 Wh/kg-material (the initial energy efficiency is 86.74%) with a retention of 1040.21 Wh/kg-material after 100 cycles at a current density of 0.2 A g^{-1}(Fig. 6f). What is more impressive that under the current density of 2000 mA g^{-1} (Fig. 6g), the doughnut-structured FeS_2@C nanorings electrode shows superior long cycle life. The initial Coulombic efficiency is 86.58%. After 500 cycles, it can still maintain the discharge capacity of 380.36 mAh g^{-1}. In order to understand the excellent electrochemical properties of the doughnut-structured FeS_2@C nanoring materials, the EIS measurements were performed before and after 100 cycles at the current density of 0.2 A g^{-1} (Fig. S6). The R_{ct} value of the doughnut-structured FeS_2@C nanoring electrode after 100th cycles is smaller than that before the cycle, which indicates the faster charge transfer in the lithium insertion/deintercalation process. In recent years, among pyrite materials used for LIBs, the doughnut-structured FeS_2@C nanoring electrode developed in this work is at a fairly high level (Table S1).It is worth noting that the capacity of FeS_2@C nanorings is close to the theoretical value of related iron sulfide, for example, 894 mA h g^{-1} for FeS_2 . The high capacity was previously reported for iron sulfides based lithium-ion storage,[47, 59-61] which is in general regarded as a result of the related synergistic effects including the formation of a polymeric gel-like film and possibly the insertion of lithium ions into interfacial storage.[60, 61] Before charge−discharge cycling there are more distinct interfaces between the core and the shell in the FeS_2@C nanorings structure. After continuous charge−discharge processes, FeS_2 could gradually convert into Li_2S and Fe^0.[60,62] The strong interfacial interactions between the core and shell enable to shorten the diffusion path of lithium ions and finally form a stable structure during cycling. Therefore, FeS_2@C nanoring exhibits excellent stability and high capacity, as well as good cycling performance.

All the above results show that the doughnut-structured FeS_2@C nanorings electrode material has the high capacity, good cycling performance and excellent rate capability performance, indicating that the doughnut-structured FeS_2@C nanorings material is a good candidate for the cathode material for LIBs. These excellent performances can be ascribed to the unique doughnut-like structure of FeS_2@C. And this structure can relieve volume expansion and capacity reduction, and more importantly, outer carbon layer can effectively improve the conductivity of electrode materials.

4. Conclusions

In summary, unique doughnut-structured FeS_2@C nanorings have been successfully synthesized through a distinctive vulcanization method, which also exhibit excellent rate capability and superior long cycle stability as the cathode electrode material for LIBs. More concretely, it shows a reversible capacity of 765.85 mAh g^{-1} after 100 cycles at a current density of 100 mA g^{-1},and an impressively ultra-long cycle life with a capacity of 380.36 mAh g^{-1} after 500 cycles at a current density of 2 A g^{-1}. It indicates that the doughnut-structured FeS_2@C nanoring

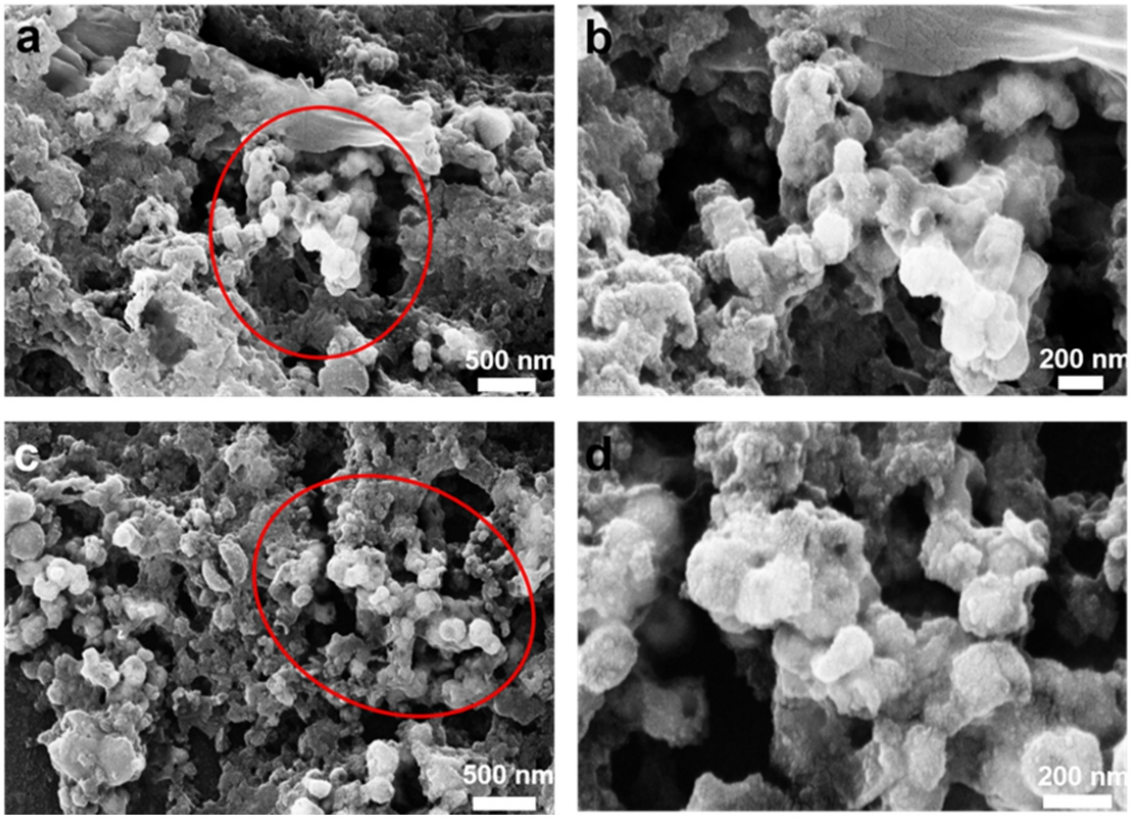

Fig. 7 (a–d)SEM images of doughnut-structured FeS_2@C nanorings electrode material after the rate capability performance test at various current rates from 100 mA g^{-1} to 2A g^{-1}.

materials can be potentially applied to high-performance LIBs. More importantly, this study provides a new idea for the preparation of new generation of sulfide electrode materials.

Financial interests statements

The authors declare no competing financial interest.

Acknowledgements

The authors are grateful for support from the National Natural Science Foundation of China (Nos.21671160), Defense Industrial Technology Development Program (JCKY2016208B012); Thousand Talents Program in Sichuan Province; Longshan Talent Program of Southwest University of Science and Technology. The data were tested by the Southwest University of Science and Technology analytical and testing center.

References

1. Y. Y. Xin and W. L. Xiong, *Adv. Energy Mater.*, 2018, **8**, 1701592.
2. Z. Li, H. B. Wu and X. W. Lou, *Energy Environ. Sci.*, 2016, **9**.
3. K. P. Wu, K. Du and G. R. Hu, *J.Mater. Chem. A*, 2018, **6**, 1057-1066.
4. Y. H. Tan, W. T. Yao, T. W. Zhang, T. Ma, L. L. Lu, F. Zhou, H. B. Yao and S. H. Yu, *ACS Nano*, 2018, **12**, 5856-5865.
5. K. Lu, Z. Y. Hu, Z. H. Xiang, J. Z. Ma, B. Song, J. T. Zhang and H. Y. Ma, *Angew. Chem.Inter. Edit.*, 2016, **55**, 10448-10452.
6. F. Zhang, C. Wang, G. Huang, D. Yin and L. Wang, *J.Power Sources*, 2016, **328**, 56-64.
7. D. Chao, C. Zhu, P. Yang, X. Xia, J. Liu, W. Jin, X. Fan, S. V. Savilov, J. Lin and J. F. Hong, *Nat. Commun.*, 2016, **7**, 12122.
8. C. Li, G. Lin, J. Tong and J. Maier, *ACS Nano*, 2011, **5**, 2930.
9. C. Li, C. Yin, L. Gu, R. E. Dinnebier, X. Mu, P. A. van Aken and J. Maier, *J. Am. Chem. Soc.*, 2013, **135**, 11425.
10. T. A. Yersak, H. A. Macpherson, S. C. Kim, V. D. Le, C. S. Kang, S. B. Son, Y. H. Kim, J. E. Trevey, K. H. Oh and C. Stoldt, *Adv. Energy Mater.*, 2013, **3**, 120-127.
11. T. Evans, D. M. Piper, S. C. Kim, S. S. Han, V. Bhat, K. H. Oh and S. H. Lee, *Adv. Mater.*, 2014, **26**, 7386-7392.
12. S. B. Son, T. A. Yersak, D. M. Piper, S. C. Kim, C. S. Kang, J. S. Cho, S. S. Suh, Y. U. Kim, K. H. Oh and S. H. Lee, *Adv. Energy Mater.*, 2013, **4**, 1300961.
13. J. M. Whiteley, S. Hafner, S. S. Han, S. C. Kim, K. H. Oh and S. H. Lee, *Adv. Energy Mater.*, 2016, **6**.
14. S. Chen, Z. Kang, X. Zhang, J. Xie, H. Wang, W. Shao, X. Zheng, W. Yan, B. Pan and Y. Xie, *ACS Cent. Sci.*, 2017, **3**, 1221-1227.
15. M. S. Whittingham, *Chem. Rev.*, 2014, **114**, 11414-11443.
16. C. Zhu, Y. Wen, P. A. Van Aken, J. Maier and Y. Yu, *Adv. Funct. Mater.*, 2015, **25**, 2335-2342.
17. J. Liu, Y. Wen, Y. Wang, P. A. V. Aken, J. Maier and Y. Yu, *Adv. Mater.*, 2014, **26**, 6025–6030.
18. D. Zhang, Y. J. Mai, J. Y. Xiang, X. H. Xia, Y. Q. Qiao and J. P. Tu, *J.Power Sources*, 2012, **217**, 229-235.
19. R. Xu, X. Zhang, C. Yu, Y. Ren, J. C. M. Li and I. Belharouak, *Chemsuschem*, 2015, **7**, 2457-2460.
20. D. N. Fronczek and W. G. Bessler, *J.Power Sources*, 2013, **244**, 183-188.
21. W. Deng, X. Zhou, Q. Fang and Z. Liu, *J.Mater. Chem. A*, 2017, **5**, 13674-13682.
22. X. Liang, Y. Liu, Z. Wen, L. Huang, X. Wang and H. Zhang, *J.Power Sources*, 2011, **196**, 6951-6955.
23. L. Wang, Y. Wang and Y. Y. Xia, *Energy Environ. Sci*, 2015, **8**, 1551-1558.
24. D. H. Wang, X. H. Xia, D. Xie, X. Q. Niu, X. Ge, C. D. Gu, X. L. Wang and J. P. Tu, *J. Power Sources*, 2015, **299**, 293-300.
25. Y. Zhu, X. Fan, L. Suo, C. Luo, T. Gao and C. Wang, *ACS Nano*, 2015, **10**, 1529-1538.
26. L. Xu, Y. Hu, H. Zhang, H. Jiang and C. Li, *ACS Sustain. Chem. Eng.*, 2016, **4**.
27. Z. Liu, T. Lu, T. Song, X. Y. Yu, X. W. D. Lou and U. Paik, *Energy Environ. Sci.*, 2017, **10**.
28. Y. Chen, X. Hu, B. Evanko, X. Sun, X. Li, T. Hou, S. Cai, C. Zheng, W. Hu and G. D. Stucky, *Nano Energy*, 2018, **46**.
29. R. Kumar, R. K. Singh, A. R. Vaz, R. Savu and S. A. Moshkalev, *ACS Appl.Mater. Inter.*, 2017, **9**.
30. G. Divyapriya, I. M. Nambi and J. Senthilnathan, *Chem. Eng. J.*, 2017, **316**, 964-977.
31. Y. Li, R. A. V. Santen and T. Weber, *J.Solid State Chem.*, 2008, **181**, 3151-3162.
32. Pablo Velásquez, Dietmar Leinen, José Pascual, R. B. ‡, „ Paula Grez, Humberto Gómez, Ricardo Schrebler, R. D. R. And, ‖ and R. Córdova ‖, *J.Phy. Chem. B*, 2005, **109**, 4977-4988.
33. S. Niu, W. Lv, G. Zhou, H. Shi, X. Qin, C. Zheng, T. Zhou, C. Luo, Y. Deng and B. Li, *Nano Energy*, 2016, **30**, 138-145.
34. C. J. Jia, L. D. Sun, F. Luo, X. D. Han, L. J. Heyderman, Z. G. Yan, C. H. Yan, K. Zheng, Z. Zhang and M. Takano, *J. Am. Chem. Soc.*, 2015, **130**, 16968-16977.
35. K. Lu, H. Zhang, S. Gao, Y. Cheng and H. Ma, *Nanoscale*, 2018, **10**, 20754-20760.
36. X. Xu, J. Liu, Z. Liu, J. Shen, R. Hu, J. Liu, L. Ouyang, L. Zhang and M. Zhu, *ACS Nano*, 2017, **11**, 9033.
37. H. He and C. Gao, *ACS Appl. Mater. Inter.*, 2010, **2**, 3201-3210.
38. K. Lu, D. Li, X. Gao, H. X. Dai, N. Wang and H. Y. Ma, *J.Mater.Chem.A*, 2015, **3**, 16013-16019.
39. K. P. Wu, D. W. Liu and Y. Tang, *Electrochim. Acta*, 2018, **263**, 515-523.
40. K. Lu, R. Jiang, X. Gao and H. Ma, *Rsc Adv.*, 2014, **4**, 52393-52401.
41. Q. Meng, H. Wan, W. K. Zhu, T. Duan and W. T. Yao, *ACS Sustain. Chem. Eng*, 2017, **6**.
42. Y. H. Tan, F. Zhou, Z. H. Huang, W. T. Yao, T. W. Zhang, H. B. Yao, L. L. Lu and S. H. Yu, *Chemelectrochem*, 2018, **5**.
43. X. Wen, X. Wei, L. Yang and P. Shen, *J.Mater.Chem. A*, 2015, **3**, 2090-2096.
44. X. Chen, Z. Wang, X. Wang, J. Wan, A. Jianwei Liu and Y. Qian, *Inorg. Chem.*, 2005, **44**, 951.
45. C. Wadia, Y. Wu, S. Gul, S. K. Volkman, J. Guo and A. P. Alivisatos, *Chem. Mater.*, 2009, **21**, 7018-7022.
46. K. N. Kudin, B. Ozbas, H. C. Schniepp, R. K. Prud'Homme, I. A. Aksay and R. Car, *Nano Lett.*, 2007, **8**, 36.
47. C. Xu, Y. Zeng, X. Rui, N. Xiao, J. Zhu, W. Zhang, J. Chen, W. Liu, H. Tan and H. H. Hng, *ACS Nano*, 2012, **6**, 4713-4721.
48. R. Tan, J. Yang, J. Hu, K. Wang, Y. Zhao and F. Pan, *Chem. Commun*, 2015, **52**, 986-989.
49. E. J. Kim and B. Batchelor, *Mater. Res. Bull*, 2009, **44**, 1553-1558.
50. J. Xu, H. Xue, X. Yang, H. Wei, W. Li, Z. Li, W. Zhang and C. S. Lee, *Small*, 2015, **10**, 4754-4759.
51. W. Qiu, J. Xia, H. Zhong, S. He, S. Lai and L. Chen, *Electrochim. Acta*, 2014, **137**, 197-205.
52. L. J. Liu, Y. Chen, Z. F. Zhang, X. L. You, M. D. Walle, Y. J. Li and Y. N. Liu, *J.Power Sources*, 2016, **325**, 301-305.
53. H. Chen, M. Q. Wang, Y. Yu, H. Liu, S. Y. Lu, S. J. Bao and M. Xu, *ACS Appl. Mater. Inter.*, 2017, **9**, 35040.
54. K. P. Wu, K. Du and G. R. Hu, *J.Mater. Chem.A*, 2018, **6**, 3444-3453.
55. J. Y. Dai, J. J. Li, Q. B. Zhang, M. Liao, T. Duan and W. T. Yao, *Mater. Lett.*, 2019, **236**, 483-486.
56. G. X. Pan, F. Cao, X. H. Xia and Y. J. Zhang, *J. Power Sources*, 2016, **332**, 383-388.
57. H. Wang, Q. Pan, Y. Cheng, J. Zhao and G. Yin, *Electrochim. Acta*, 2009, **54**, 2851-2855.
58. L. Li, M. Cabán-Acevedo, S. N. Girard and S. Jin, *Nanoscale*, 2014, **6**, 2112.
59. C. D. Wang, M. H. Lan, Y. Zhang, H. D. Bian, M. F. Yuen, K. K. Ostrikov, J. J. Jiang, W. J. Zhang, Y. Y. Li and J. Lu, *Green Chem.*, 2016, **18**, 3029-3039.
60. W. Huang, S. Li, X. Cao, C. Hou, Z. Zhang, J. Feng, L. Ci, P. Si and Q. Chi, *ACS Sustain. Chem. Eng.*, 2017, **5**, 5039-5048.
61. E. Liu, J. Wang, C. Shi, N. Zhao, C. He, J. Li and J. Z. Jiang, *ACS Appl. Mater. Inter.*, 2014, **6**, 18147-18151.
62. Q. Zhang, J. Liao, M. Liao, J. Dai, H. Ge, T. Duan, W. Yao, *Appl. Sur. Sci.*, 2019, **473**, 799-806.